Supplement of Clim. Past, 18, 1963–1982, 2022
https://doi.org/10.5194/cp-18-1963-2022-supplement

Climate of the Past
Open Access

Supplement of

Clumped-isotope-derived climate trends leading up to the end-Cretaceous mass extinction in northwestern Europe

Heidi E. O'Hora et al.

Correspondence to: Sierra V. Petersen (sierravp@umich.edu)

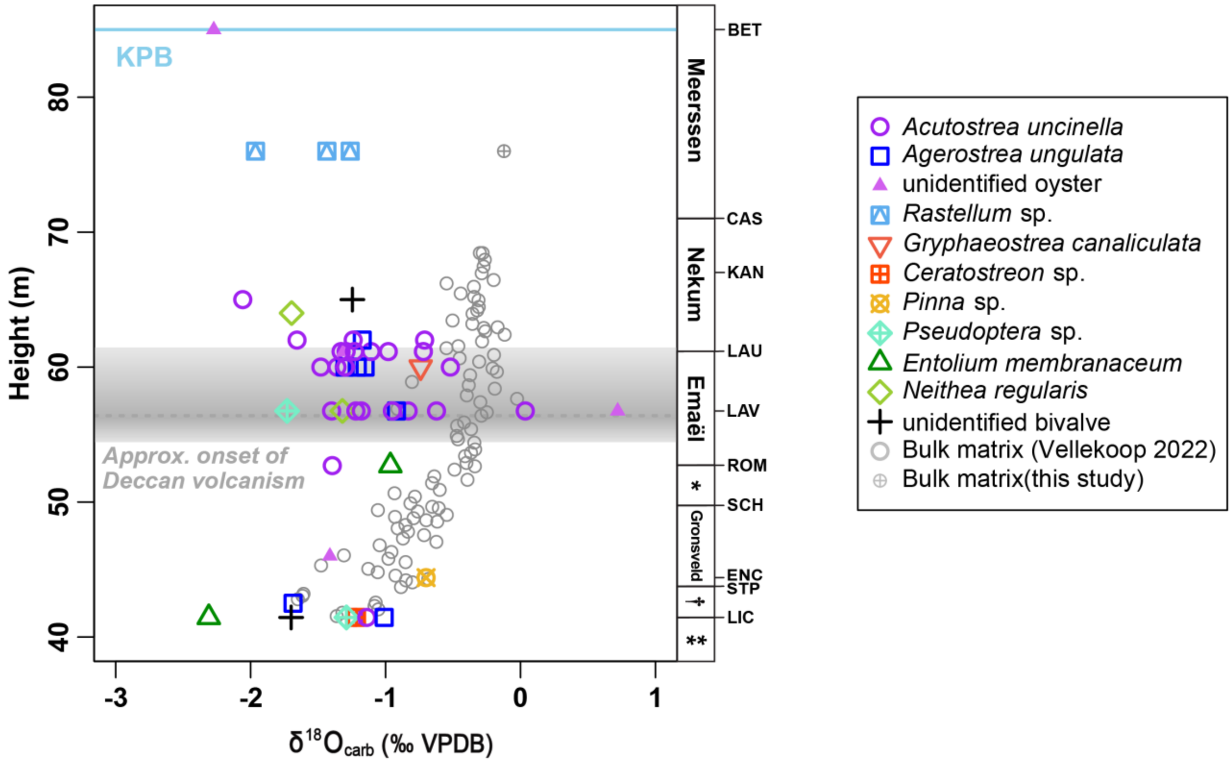

Figure S1: Oxygen isotope values of shell specimens, divided by species, compared to bulk carbonate. Bulk carbonate $\delta^{18}O$ data from Vellekoop et al. (2022) and this study (one point) shown in dark grey. K-Pg boundary at 66.0 Ma (blue line) and approximate onset of the main phase of Deccan Traps eruptions (grey dotted line and grey shading) at 66.413 ± 0.067 Ma (Sprain et al., 2019), converted into depth. Member names and horizon abbreviations are labeled along right side of figure. *Schiepersberg Member; †Valkenberg Member; ⁑Laneye Member of the underlying Gulpen Formation. Samples that fail screening criteria are not included here. No apparent species-related offsets are seen in oxygen isotopes. Fossil shells are generally 0.5–1 ‰ lower than bulk matrix carbonated. Error on $\delta^{18}O$ data is not shown, but is typically ~0.1‰, which is similar to the size of the symbol.

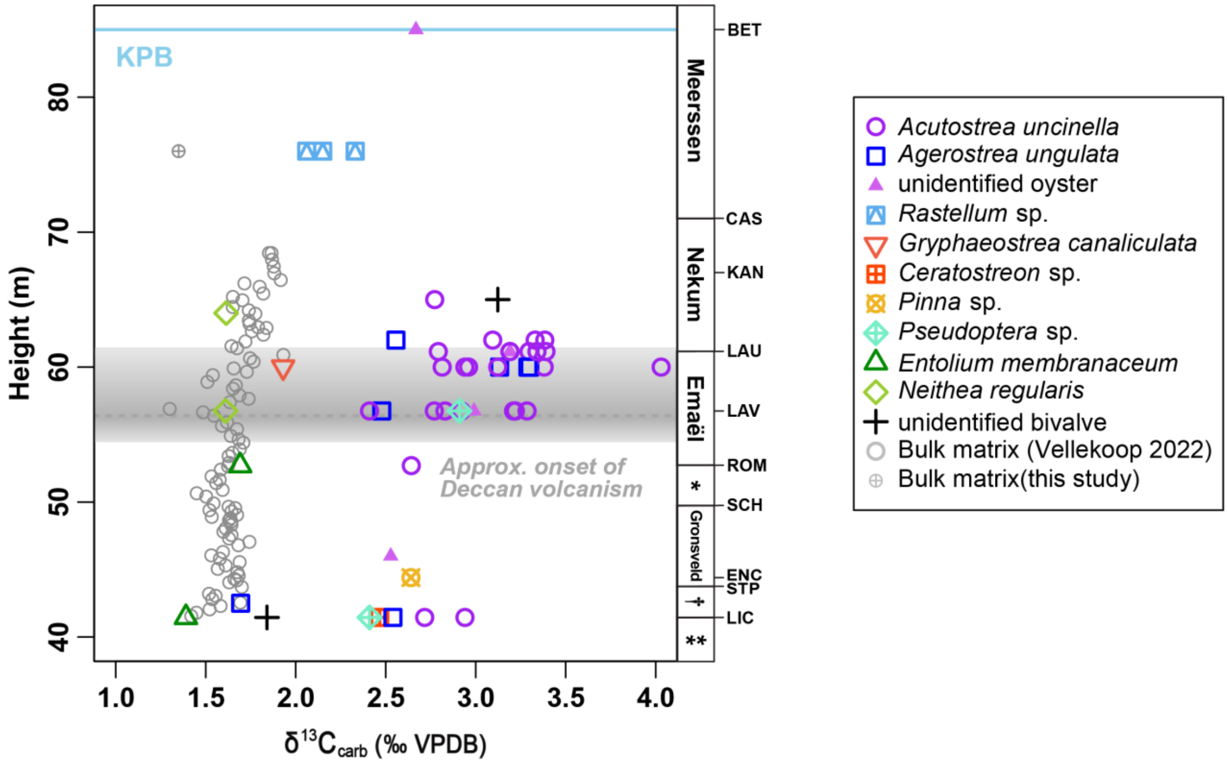

Figure S2: Carbon isotope values of shell specimens, divided by species, compared to bulk carbonate. Bulk carbonate $\delta^{13}C$ data from Vellekoop et al. (2022) and this study (one point) shown in dark grey. K-Pg boundary at 66.0 Ma (blue line) and approximate onset of the main phase of Deccan Traps eruptions (grey dotted line and grey shading) at 66.413 ± 0.067 Ma (Sprain et al., 2019), converted into depth. Member names and horizon abbreviations are labeled along right side of figure. *Schiepersberg Member; †Valkenberg Member; ⁑Laneye Member of the underlying Gulpen Formation. Samples that fail screening criteria are not included here. Apparent species-related offsets are seen in carbon isotopes for *Entollium membranaceum* and *Neithea regularis*, which are ~1 ‰ lower than other oyster species. These two species are from a different order than all the other taxa (Pectinidae vs. Ostridae for most others), which may explain this deviation. Fossil oyster shells are generally 1–1.5 ‰ higher than bulk matrix carbonate. Error on $\delta^{13}C$ data is not shown, but is typically <0.1‰, which is similar to or smaller than the size of the symbol.

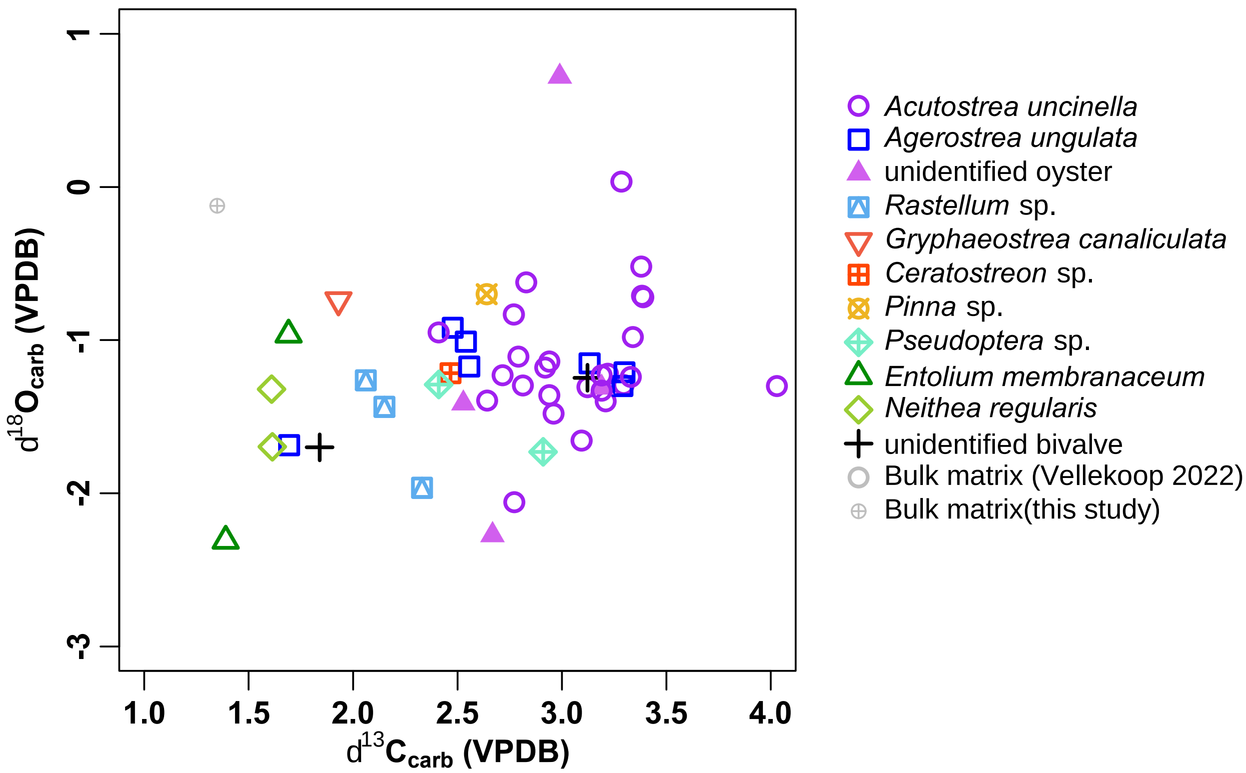

Figure S3: Carbon isotopic composition vs. oxygen isotopic composition in well-preserved shells and bulk matrix. All species (and bulk matrix) cover a similar range in $\delta^{18}O_{carb}$ but show differences in in $\delta^{13}C_{carb}$. In particular, the two species in order Pectinidae (*Neithea regularis* and *Entolium membranaceum*) display lower $\delta^{13}C$ than other species in order Ostridae. Is it difficult to separate the influences of species and age in certain cases such as in the intermediate $\delta^{13}C$ values shown in *Rastellum* sp.. *Rastellum* sp. only occurs in the Meerssen Member and nowhere else and no other species occur in that member for direct cross-comparison. Error bars of 1sd (not shown) are generally less than 0.1 ‰ in $\delta^{13}C$ and 0.2 ‰ in $\delta^{18}O$.

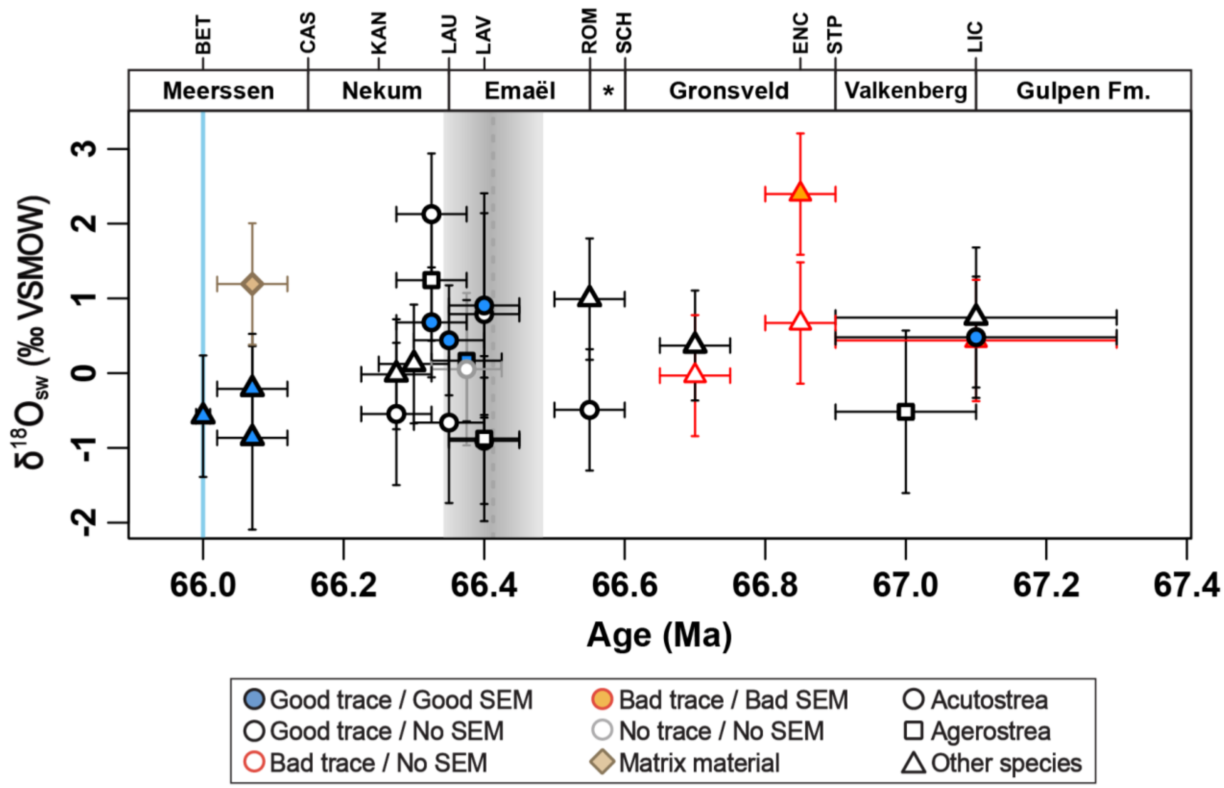

Figure S4: Reconstructed seawater oxygen isotopic composition through time. Comparable to Fig. 5 in the main text, except plotting $\delta^{18}O_{sw}$ instead of temperature. Highest values seen in the basal Nekum Member at 66.375 Ma, aligning with the warming peak in Fig. 5. Samples shown in red (n=4) did not pass screening thresholds and were not included in further interpretation. Error bars represent the larger of either the internal or long-term 1SE (see text). Onset of the main Deccan Traps eruptions (grey shading) at 66.413 ± 0.067 Ma (Sprain et al., 2019). Member names and horizon abbreviations are labeled across top of figure (see Fig. 2). *Schiepersberg Member.

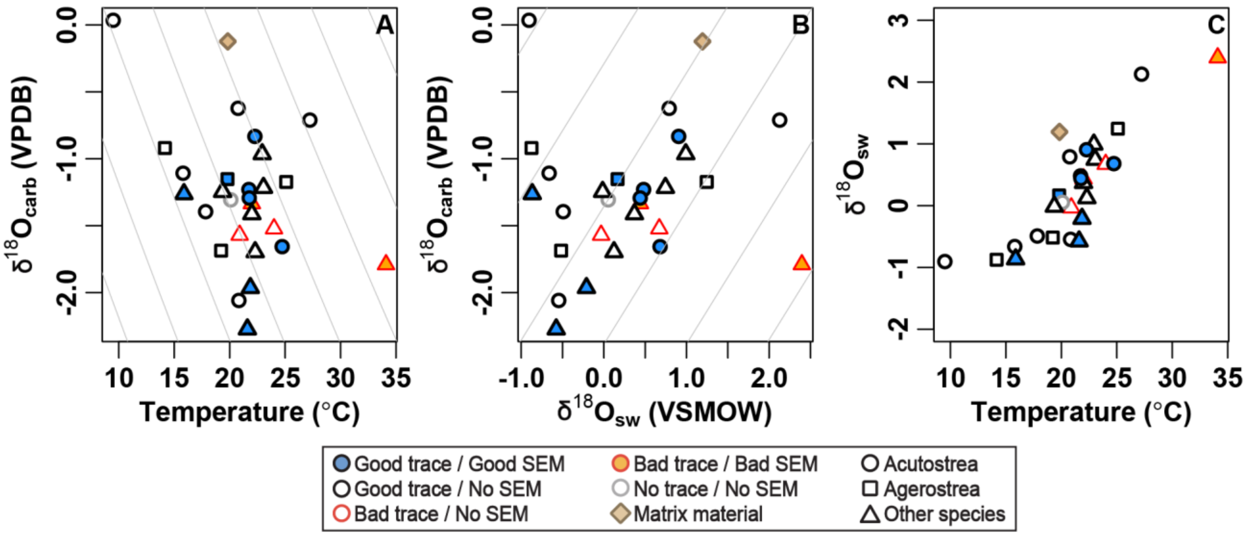

Figure S5: Covariation of oxygen isotopic composition of carbonate and water with temperature. (a) Temperature vs. $\delta^{18}O_{carb}$. Grey lines are lines of constant $\delta^{18}O_{sw}$, varying from -3 ‰ on the bottom left to +4 ‰ VSMOW at the top right with 1 ‰ spacing, calculated using the relationship of Kim and O'Neil (1997). (b) $\delta^{18}O_{sw}$ vs. $\delta^{18}O_{carb}$. Grey lines are lines of constant temperatures, varying from 10 °C in the top left to 35 °C in the bottom right with 5 °C spacing. (c) Temperature vs. $\delta^{18}O_{sw}$. Because neither temperature nor $\delta^{18}O_{sw}$ appears to be the sole driver of $\delta^{18}O_{carb}$ (no strong linear relationship in (a) or (b)), calculations result in a visible correlation between temperature and $\delta^{18}O_{sw}$. Although the quantitative fit would be driven primarily by a small number of points near the extremes, the qualitative relationship is clearly present in the temporal evolution, so we interpret this as covariation in temperature and $\delta^{18}O_{sw}$ over million-year timescales as a result of changing ice volume, sea level, and ocean circulation (see text). Error bars are not shown for clarity, but are generally ± 3–4 °C on temperature, ± 0.7–1.0 ‰ on $\delta^{18}O_{sw}$, and ± 0.1–0.2 ‰ on $\delta^{18}O_{carb}$.

Table S1: Published paleotemperature data for other studies reconstructing Maastrichtian marine temperatures, sorted by paleolatitude. Data from this study is bold. All paleolatitudes were determined either directly from each study (if given) or via www.paleolatitude.org (van Hinsbergen et al., 2015). All temperatures are in degrees Celsius. The average temperature from sites located between 30–50° N show an average temperature of 19.8 ± 5.2 °C (n = 23 studies, black rows). Other rows from just outside this latitude range, or from a similar southern hemisphere latitude, are shown in itallics for comparison but are not used in this calculation.

Study	**Proxy Type**	**Locality**	**Approx. Age**	**Paleolat.**	**Avg. Temp.**
Dennis et al. (2013)	*Clumped isotopes of gastropods, nautiloid, ammonites, belemnite, clams*	*Hell Creek, MT, USA*	*67.0–73.5 Ma*	*53*	*20.5*
Tobin et al. (2014)	*Clumped isotopes of gastropods, bivalves*	*Hell Creek, MT, USA*	*65.2–67.1 Ma*	*53*	*25.9*
Zhang et al. (2018)	*Clumped isotopes of paleosol carbonates*	*Songliao Basin, China*	*65.0–76.0 Ma*	*52*	*17.0*
Meyer et al. (2019)	Clumped isotopes of belemnites, bivalves	Scania, Sweden	69.2–72.3 Ma	46	13.9
Tagliavento et al. (2019)	Clumped isotopes of coccolithic chalk	Danish Basin, Denmark	Late Campanian to Maastrichtian	46	24.5
Maestas et al. (2003)	Planktic foraminiferal $\delta^{18}O$	San Antonio Del Mar, Baja California	Late Campanian to Maastrichtian	42	19.5
Pucéat et al. (2007)	Phosphate $\delta^{18}O$ of fish teeth	Nasilov, Poland	66.0 Ma	40	14.6
Pucéat et al. (2007)	Phosphate $\delta^{18}O$ of fish teeth	South-Central NJ, USA	Mid to late Maastrichtian	40	14.4
This study	**Clumped isotopes of oysters, clams, scallops**	**SE Netherlands & NE Belgium**	**66.0–67.4 Ma**	**40**	**19.2**
Vellekoop et al. (2016)	TEX_{86}	Monmouth County, NJ, USA	65.6–66.8 Ma	37	26.1
Meyer et al. (2018)	Clumped isotopes of oysters	Monmouth County, NJ, USA	70.7 Ma	37	13.8
Esmeray-Senlet et al. (2015)	Planktic foraminiferal $\delta^{18}O$	Bass River, NJ, USA	66.1–66.6 Ma	36	21.7
Woelders et al. (2018)	Planktic foraminiferal $\delta^{18}O$	Bass River, NJ, USA	66.0–66.3 Ma	36	25.2
Woelders et al. (2018)	TEX_{86}	Bass River, NJ, USA	66.1–66.5 Ma	36	27.8
Woelders et al. (2018)	Planktic foraminiferal Mg/Ca	Bass River, NJ, USA	66.1–66.4 Ma	36	22.0
Meyer et al. (2018)	Clumped isotopes of oysters, clams, gastropod	Western TN, USA	73.5 Ma	36	21.5
Vellekoop et al. (2014)	TEX_{86}	Brazos River, TX, USA	65.7–66.3 Ma	35	29.8
Meyer et al. (2018)	Clumped isotopes of oysters, clams	Moscow Landing, AL, USA	65.0–74.0 Ma	33	22.1
Meyer et al. (2018)	Clumped isotopes of oysters, clams, belemnite	Burches Ferry, SC, USA	71.4 Ma	33	20.6
Huber et al. (1995)	Planktic foraminiferal $\delta^{18}O$	Blake Nose, North Atlantic Ocean	Maastrichtian	31	18.6
Berggren and Norris (1997)	Planktic foraminiferal $\delta^{18}O$	DSDP 384, North Atlantic Ocean	64.9–66.2 Ma	31	9.8
Frank and Arthur (1999)	Planktic foraminiferal $\delta^{18}O$	Blake Nose, North Atlantic Ocean	Maastrichtian	31	21.1
Huber et al. (2002)	Planktic foraminiferal $\delta^{18}O$	Blake Nose, North Atlantic Ocean	66.0 Ma	31	18.1

Friedrich et al. (2004)	Planktic foraminiferal $\delta^{18}O$	Blake Nose, North Atlantic Ocean	69.6–71.3 Ma	31	19.6
MacLeod et al. (2005)	Planktic foraminiferal $\delta^{18}O$	Blake Nose, North Atlantic Ocean	Late Maastrichtian	31	21.4
Zakharov et al. (2006)	Planktic foraminiferal $\delta^{18}O$	Blake Nose, North Atlantic Ocean	Maastrichtian	31	18.3
Hull et al. (2020)	Bulk carbonate $\delta^{18}O$	IODP U1403, North Atlantic Ocean	66.0–68.8 Ma	31	11.2
Li and Keller (1998)	*Planktic foraminiferal* $\delta^{18}O$	*DSDP 525, South Atlantic Ocean*	*66.0–66.5 Ma*	*-40*	*15.0*
Kroon et al. (2007)	*Bulk carbonate* $\delta^{18}O$	*ODP 1262, South Atlantic Ocean*	*65.0–67.1 Ma*	*-41*	*9.9*
Birch et al. (2016)	*Planktic foraminiferal* $\delta^{18}O$	*ODP 1262, South Atlantic Ocean*	*66.0–66.5 Ma*	*-41*	*14.5*
Woelders et al. (2017)	TEX_{86}	*Bajada del Jagüel, Argentina*	*64.0–66.7 Ma*	*-43*	*27.2*

Table S2: Age model used in this study, from Vellekoop et al. (2022). Samples from GSG and CRB Romontbos quarry shown for comparison. Bold indicates horizons where samples were collected/analyzed, following Fig. 2.

Horizon or Member	Age (Ma)	Error (Ma)	Height in Column (m)
Lichtenberg Hz	**67.1**	**0.2**	**41.45**
Valkenburg Mbr	**~67.0**	**0.1**	**~42.5**
St. Pieter Hz	66.9	0.1	43.75
ENCI Hz	**66.85**	**0.05**	**44.4**
Gronsveld Mbr	~66.70	0.05	~46
Schiepersberg Hz	66.6	0.05	49.75
Rotmonbos Hz	**66.55**	**0.05**	**52.7**
Lava Hz	**66.4**	**0.05**	**56.75**
Emael Mbr (top)	**66.375**	**0.05**	**~60**
Laumont Hz	**66.35**	**0.05**	**61.15**
Nekum Mbr (base)	**66.325**	**0.05**	**~62**
Nekum Mbr (mid)	**66.3**	**0.05**	**~64**
Nekum Mbr (CBR)	**~66.275**	**0.05**	**~65**
Kanne Hz	66.25	0.05	67.0
Caster Hz	66.15	0.05	~71
Meerssen Mbr (top/mid)	**66.07**	**0.05**	**~76**
Berg en Terblijt Hz (GSG)	**66.0**	**0.01**	**~85**

Table S3: Preservation assessment report. Sample Name formatted as FORM-SpeX where FORM = 3–4 capital letters corresponding to the formation, Spe = 3–4 letter abbreviation of the species or genera name, and X = A, B, C, etc. identifier if multiple shells of the same species occurred from the same horizon. Trace element concentrations were screened at a level of 100 ppm for Mn and 2050 for Fe. Shells imaged under Scanning Electron Microscope (SEM) were rated on a scale of 0 (none) to 3 (extensive) for both dissolution and secondary growth. The final rating on the rightmost column combines these two methods of screening. Any sample that failed either one or the other screening method was excluded from analysis.

Sample No.	Sample ID	Sample Name	Mg (ppm)	Mn (ppm)	Fe (ppm)	Sr (ppm)	SEM Diss.	SEM SG	SEM Both	P. Index
1	JV-NL-001	LIC-Psop	1780	69	1009	770	-	-	-	GT/NA
2	JV-NL-002	LIC-Pycn	4027	86	4441	983	0	2	BAD	Fe/BAD
3	JV-NL-003	LIC-AcutA	1617	37	1718	899	0	1	GOOD	GT/GOOD
4	JV-NL-004	LIC-Gry	1412	42	881	726	-	-	-	GT/NA
5	JV-NL-005	LIC-AcutB	1518	44	228	780	-	-	-	GT/NA
6	JV-NL-006	LIC-Ager	1693	59	390	779	-	-	-	GT/NA
7	JV-NL-007	LIC-biv	3540	89	217	670	-	-	-	GT/NA
8	JV-NL-008	LIC-Ento	2676	88	646	646	-	-	-	GT/NA
8.59	JV-NL-0059	VAL-Ager	2616	89	1102	808	-	-	-	GT/NA
9	JV-NL-009	ENC-Pinna	3783	23	475	1082	-	-	-	GT/NA
10	JV-NL-0010	ENC-BivA	4956	105	4345	782	-	-	-	FeMn/NA
11	JV-NL-0011	ENC-BivB	4708	128	3355	952	0	3	BAD	FeMn/BAD
11.6	JV-NL-0060	GRO-Biv	3163	210	713	1057	-	-	-	Mn/NA
11.61	JV-NL-0061	GRO-OstA	598	25	383	245	-	-	-	GT/NA
11.62	JV-NL-0062	GRO-Ost	1379	55	371	1120	-	-	-	GT/NA
12	JV-NL-0012	ROT-Acut	2374	50	295	1071	-	-	-	GT/NA
13	JV-NL-0013	ROT-Ento	4577	73	1032	949	-	-	-	GT/NA
14	JV-NL-0014	LAV-AcutG	1750	30	597	714	0	0	GOOD	GT/GOOD
15	JV-NL-0015	LAV-NeitA	2404	67	3201	1760	-	-	-	Fe/NA
16	JV-NL-0016	LAV-NeitB	2263	42	711	1421	1	0	GOOD	GT/GOOD
17	JV-NL-0017	LAV-AcutA	3324	69	1084	1175	-	-	-	GT/NA
18	JV-NL-0018	LAV-AcutB	3074	59	286	821	0	0	GOOD	GT/GOOD
19	JV-NL-0019	LAV-AcutC	964	24	595	661	-	-	-	GT/NA
20	JV-NL-0020	LAV-AcutD	1979	61	636	785	-	-	-	GT/NA
21	JV-NL-0021	LAV-AcutE	2604	48	689	1034	-	-	-	GT/NA
22	JV-NL-0022	LAV-AcutF	3873	78	96	494	-	-	-	GT/NA
23	JV-NL-0023	LAV-Ost	3365	76	599	1394	-	-	-	GT/NA
24	JV-NL-0024	LAV-Ager	2132	49	1561	921	-	-	-	GT/NA
25	JV-NL-0025	LAV-Psop	1664	48	269	916	-	-	-	GT/NA
26	JV-NL-0026	EMAU-AgerA	1034	36	376	877	-	-	-	GT/NA
27	JV-NL-0027	EMAU-AgerB	1845	40	578	851	0	2	BAD	GT/BAD
28	JV-NL-0028	EMAU-AgerC	1156	40	2013	989	1	0	GOOD	GT/GOOD
29	JV-NL-0029	EMAU-AcutA	-	-	-	-	-	-	-	NA/NA
30	JV-NL-0030	EMAU-AcutB	1174	28	863	871	-	-	-	GT/NA
31	JV-NL-0031	EMAU-AcutC	2195	60	2423	628	-	-	-	GT/NA
32	JV-NL-0032	EMAU-AcutD	1196	35	103	870	-	-	-	GT/NA
33	JV-NL-0033	EMAU-AcutE	1880	28	348	859	-	-	-	GT/NA
34	JV-NL-0034	EMAU-AcutF	2385	58	1142	825	0	0	GOOD	GT/GOOD
35	JV-NL-0035	EMAU-AgerD	1815	28	176	778	-	-	-	GT/NA
36	JV-NL-0036	EMAU-AcutG	1557	37	1515	1055	0	0	GOOD	GT/GOOD
37	JV-NL-0037	EMAU-AcutH	2127	19	262	828	-	-	-	GT/NA
38	JV-NL-0038	EMAU-Cer	1745	35	512	1137	-	-	-	GT/NA
39	JV-NL-0039	LAU-Unoy	1953	57	711	848	3	0	OK	GT/OK
40	JV-NL-0040	LAU-AcutA	2604	100	7151	848	-	-	-	FeMn/NA
41	JV-NL-0041	LAU-AcutB	1948	42	269	953	-	-	-	GT/NA
42	JV-NL-0042	LAU-AcutC	888	38	2008	946	-	-	-	GT/NA
43	JV-NL-0043	LAU-AcutD	1118	48	1907	996	-	-	-	GT/NA
44	JV-NL-0044	LAU-AcutE	1223	39	166	783	0	0	GOOD	GT/GOOD
45	JV-NL-0045	LAU-AcutF	728	49	1014	633	-	-	-	GT/NA
46	JV-NL-0046	LAU-AcutG	1484	36	1163	831	0	1	GOOD	GT/GOOD
47	JV-NL-0047	NEKB-AcutA	1170	25	724	870	-	-	-	GT/NA
48	JV-NL-0048	NEKB-AcutBC	1769	36	249	800	0	1	GOOD	GT/GOOD
49	JV-NL-0049	NEKB-AcutD	1365	17	225	731	1	0	GOOD	GT/GOOD
50	JV-NL-0050	NEKB-AcutE	2482	42	2069	896	3	2	BAD	GT/BAD
51	JV-NL-0051	NEKB-AcutF	2175	46	3609	759	-	-	-	Fe/NA
52	JV-NL-0052	NEKB-Ager	1982	60	387	958	-	-	-	GT/NA
53	JV-NL-0053	NEK-Neit	2677	46	436	950	1	2	BAD	GT/BAD
54	JV-NL-0054	NEK-Acut	2983	45	345	828	3	2	BAD	GT/BAD
54.63	JV-NL-0063	NEK-NeitB	2122	39	286	1507	-	-	-	GT/NA
54.94	JV-BE-004	CBR-Acut	2362	31	482	1069	-	-	-	GT/NA
54.95	JV-BE-005	CBR-Biv	2292	21	226	996	-	-	-	GT/NA
55	JV-NL-0055	MEER-RasA	1831	41	270	722	0	0	GOOD	GT/GOOD
56	JV-NL-0056	MEER-RasB	1195	35	843	774	0	0	GOOD	GT/GOOD
57	JV-NL-0057	MEER-RasC	1266	31	410	828	-	-	-	GT/NA
57.1	JV-NL-0057m	MEER-mat	5886	60	664	520	-	-	-	GT/NA
58	JV-NL-0058	MEER-RasD	1964	41	617	865	-	-	-	GT/NA
58.1	SP-NL-001	GCAV-oystA	862	61	245	886	1	1	GOOD	GT/GOOD

Table S4: Summary of in-house carbonate standards. CM = Calcitic Carrara Marble. **OO =** Aragonitic ooid mixture, collected from Joulter's Cay, Bahamas, with a mean annual temperature of ~22 °C (which would correspond to a $\Delta_{47\text{-CDES25}}$ value of 0.697 ‰). **CORS =** Mixed aragonitic standard made of pulverized zooxanthellate coral rubble from Hawaii (Rosenheim et al., 2013). CORS is not expected to correlate to a modern Hawaiian mean annual temperature due to coral vital effects. Previously reported value is 0.737 ± 0.005 ‰ (1 SE, N=21), using Santrock/Gonfiantini parameters and older acid fractionation factors (see Rosenheim et al., 2013). **Pica =** Aragonitic modern *Cittarium pica* shell, crushed in total, collected from Bermuda, which has a mean annual temperature of ~23 °C (which would correspond to a $\Delta_{47\text{-CDES25}}$ value of 0.695 ‰). The heavier value here may represent vital effects in this gastropod species. **Ice =** Aragonitic modern *Arctica islandica* from the north coast of Iceland (Hvitserkur), crushed in total. This region of the Iceland Sea has a mean annual temperature of ~4 °C and a summertime peak of ~9.5 °C. Because the shell was crushed in total and shell carbonate is likely to be volumetrically weighted towards summertime growth, we expect a temperature somewhere between 4 ($\Delta_{47\text{-CDES25}}$ value of 0.757 ‰) and 9.5 °C ($\Delta_{47\text{-CDES25}}$ value of 0.737 ‰). Errors shown here are ± 1 sd in all cases. Long-term standard deviation of 0.020 ‰ in Δ_{47} for the MAT253 is calculated as the mean of 1sd of CM, OO, and Pica. Long-term standard deviation of 0.018 ‰ in Δ_{47} for the Nu Perspective is calculated as the mean of 1sd of all five standards. On the MAT253, sessions in 2016 and 2017 included only CM and OO. CORS was added in 2017.

Standard	**Kiel**	**MAT 253**		**Nu Perspective**	
	Calibration (2014, 2019)	**Long Term** (2015, 2018–19)	**These Sessions** (2016–17, 2019–20)	**Long Term** (Jul–Dec 2020)	**These Sessions** (2021A, 2022A)
CM	(N=17)	(N=27)	(N=18)	(N=77)	(N=18)
$\Delta_{47\text{-CDES25}}$		0.396 ± 0.024	0.398 ± 0.023	0.4066 ± 0.018	0.395 ± 0.018
$\delta^{18}O$	-2.16 ± 0.09	-2.05 ± 0.29	-2.03 ± 0.16	-2.16 ± 0.07	-2.21 ± 0.13
$\delta^{13}C$	2.05 ± 0.04	1.89 ± 0.09	1.92 ± 0.05	2.02 ± 0.021	2.03 ± 0.05
OO*	(N=8)	(N=23)	(N=15)	(N=35)	(N=18)
$\Delta_{47\text{-CDES25}}$		0.683 ± 0.022	0.700 ± 0.029	0.6864 ± 0.015	0.679 ± 0.029
$\delta^{18}O$	-0.16 ± 0.09	-0.06 ± 0.18	0.23 ± 0.16	-0.02 ± 0.07	0.05 ± 0.17
$\delta^{13}C$	4.77 ± 0.09	4.72 ± 0.09	4.76 ± 0.08	4.87 ± 0.03	4.89 ± 0.06
CORS	(N=5)	(N=12)	(N=7)	(N=38)	(N=3)
$\Delta_{47\text{-CDES25}}$		0.723 ± 0.014	0.713 ± 0.045	0.7243 ± 0.016	0.715 ± 0.011
$\delta^{18}O$	-4.07 ± 0.08	-4.10 ± 0.14	-3.84 ± 0.11	-4.02 ± 0.06	-4.11 ± 0.07
$\delta^{13}C$	-3.64 ± 0.09	-3.70 ± 0.06	-3.68 ± 0.09	-3.64 ± 0.04	-3.62 ± 0.03
Pica				(N=67)	(N=15)
$\Delta_{47\text{-CDES25}}$				0.7072 ± 0.023	0.701 ± 0.014
$\delta^{18}O$				0.52 ± 0.06	0.44 ± 0.10
$\delta^{13}C$				3.35 ± 0.03	3.33 ± 0.05
Ice				(N =30)	(N=20)
$\Delta_{47\text{-CDES25}}$				0.7409 ± 0.011	0.727 ± 0.019
$\delta^{18}O$				2.08 ± 0.08	2.04 ± 0.15
$\delta^{13}C$				2.19 ± 0.03	2.20 ± 0.06

*A new batch of Ooids was created for the Nu, and values appear to differ slightly from the original batch measured on the Kiel and the MAT 253.